Measurement of the spatial polarization distribution of circularly polarized gamma rays produced by inverse Compton scattering

Yoshitaka Taira,[1,2,*] Shunsuke Endo,[3,4] Shiori Kawamura,[4] Taro Nambu,[4] Mao Okuizumi,[4] Toshiyuki Shizuma,[5] Mohamed Omer,[6,†] Heishun Zen,[7] Yasuaki Okano,[1] and Masaaki Kitaguchi[4,8]

[1]*Institute for Molecular Science, National Institutes of Natural Sciences, Okazaki 444-8585, Japan*
[2]*School of Physical Sciences, The Graduate University for Advanced Studies (SOKENDAI), Okazaki 444-8585, Japan*
[3]*Nuclear Data Center, Japan Atomic Energy Agency, Tokai 319-1195, Japan*
[4]*Department of Physics, Nagoya University, Nagoya 464-8602, Japan*
[5]*National Institutes for Quantum Science and Technology, Tokai 319-1106, Japan*
[6]*Integrated Support Center for Nuclear Nonproliferation and Nuclear Security, Japan Atomic Energy Agency, Tokai 319-1195, Japan*
[7]*Institute of Advanced Energy, Kyoto University, Uji 611-0011, Japan*
[8]*Kobayashi-Maskawa Institute, Nagoya University, Nagoya 464-8602, Japan*

(Received 13 January 2023; revised 24 April 2023; accepted 22 May 2023; published 2 June 2023)

Inverse Compton scattering of polarized laser photons by energetic electrons is an excellent method to generate polarized gamma rays. A 100% polarized laser can generate 100% polarized gamma rays, but polarization varies depending on the scattering angle of the gamma rays. In this study, we experimentally measure the spatial polarization distribution of circularly polarized gamma rays using a magnetized iron that can measure the circular polarization of MeV gamma rays. Measurements of the asymmetry of gamma-ray transmission relative to the magnetized iron at each scattering angle clearly show that gamma rays are circularly polarized near the central axis, and they change from circular to linear polarization as the scattering angle increases. A simple way to obtain highly polarized gamma rays is to use a collimator that transmits only the central axis of the gamma rays with such polarization characteristics. Polarized gamma rays are, indeed, generated by 90° collisional inverse Compton scattering between an electron beam and a circularly polarized laser.

DOI: 10.1103/PhysRevA.107.063503

I. INTRODUCTION

Polarized gamma rays play important roles in fundamental physics such as nuclear physics and high-energy physics. Linearly polarized gamma rays can be used for the unambiguous determination of parity quantum numbers of resonantly excited states in nuclear photon scattering measurements [1] and for measurements of the ϕ-$\Lambda(1520)$ interference effect in the $\gamma p \to K^+K^-p$ reaction [2]. Circularly polarized gamma rays, which have a well-defined value of helicity, interact with the particle spin. They are used for the cross-section measurement of the spin-2/3 and spin-1/2 photon absorption [3], the investigation of parity nonconservation in nuclei [4], and the production of spin-polarized positrons [5,6].

In the electron-accelerator-based method, circularly polarized gamma rays are generated into two ways: by bremsstrahlung of longitudinally polarized electrons [3] and by inverse Compton scattering using circularly polarized lasers [7]. During inverse Compton scattering, high-energy gamma rays are produced by the collision of laser photons with high-energy electrons. Gamma rays produced by inverse Compton scattering have been developed since the 1960s using radio-frequency (rf) accelerated electron beams [8,9]. Recently, laser-accelerated electron beams have also been used [10,11].

The spatial intensity distribution of scattered gamma rays varies with polarization; circularly polarized gamma rays show an azimuthally symmetric spatial distribution, whereas that of linearly polarized gamma rays is azimuthally asymmetric [12–15]. Moreover, the polarization of gamma rays depends on the scattering angle θ; using a 100% circularly polarized laser, gamma rays are almost 100% circularly polarized near the central axis of the gamma rays. However, the degree of circular polarization decreases with the increase of scattering angle. At the angle of $\theta = 1/\gamma$, where γ is the Lorentz factor of an electron, polarization changes to linear. In the outer region of $\theta > 1/\gamma$, polarization changes to circular polarization with helicity opposite to that of the central region. As the energy of a gamma ray is determined by the scattering angle, the change in polarization with the scattering angle can be replaced by its energy. The calculated results for the degree of polarization of circularly polarized gamma rays were reported in [15–25].

Based on Ref. [7], the degree of circular polarization of the high-energy component of gamma rays varies with the polarization of the incident laser. However, to our knowledge,

*yostaira@ims.ac.jp
†Permanent address: Physics Department, Faculty of Science, Assiut University, Assiut 71516, Egypt.

there are no results showing that the spatial polarization distribution of circularly polarized gamma rays has been measured. In circularly polarized undulator radiation, where physical scattering is similar to inverse Compton scattering, the spatial polarization distribution of the generated 400-nm radiation varies with the scattering angle [26].

In this paper, we report results of measurements of the spatial polarization distribution of circularly polarized gamma rays generated by inverse Compton scattering. This measurement was conducted at the ultraviolet synchrotron orbital radiation (UVSOR)-III facility. Similar to the method performed in Ref. [7], the polarization of gamma rays was measured on the basis of the asymmetry of the transmission of the gamma rays through magnetized iron. Furthermore, the spatial polarization distribution of circularly polarized gamma rays is measured by scanning a 1-mm-diameter collimator in one direction.

Understanding the spatial polarization distribution of circularly polarized gamma rays is important, particularly for the following applications. (i) At UVSOR-III, gamma-ray-induced positron annihilation spectroscopy using linearly polarized ultrashort pulsed gamma rays was developed [27]. In the near future, spin-polarized positron annihilation spectroscopy using circularly polarized gamma rays will be developed. These spin-polarized positrons are a suitable tool for obtaining information about the electron spin around defects inside a magnetic material [28]. The generation of highly polarized positrons from highly polarized gamma rays [29] promotes the sensitive measurement of the asymmetry of the positron lifetime and the energy spectrum of annihilation gamma rays due to the reversal of positron spin orientation. The experimental measurement of the spatial polarization distribution of circularly polarized gamma rays can be useful in determining the region where gamma rays are spatially collimated, and only highly polarized gamma rays are used. (ii) As the scattering angle and energy of inverse-Compton-scattered gamma rays are clearly correlated, collimation provides quasi-monochromatic and highly polarized gamma rays with an energy spread of a few percent. This feature is useful for nuclear physics experiments and for the evaluation of gamma-ray detectors, including Compton cameras. (iii) An intense laser generates high-order harmonic gamma rays because of the nonlinear effect of inverse Compton scattering. As circularly polarized high-order harmonic gamma rays form helical wave fronts and carry orbital angular momentum [24], understanding the spatial polarization distribution of gamma rays is necessary.

Inverse Compton scattering of circularly polarized lasers has been used to measure the polarization of transversely polarized high-energy electron beams [30]. In this paper, we investigate inverse Compton scattering of unpolarized electrons and circularly polarized lasers.

II. CALCULATION

A. Gamma-ray energy of inverse Compton scattering

In the experiment, circularly polarized gamma rays are generated by 90° collisions between the high-energy electron beam and circularly polarized laser. Thus, 90° collisions are considered in the following theoretical equations.

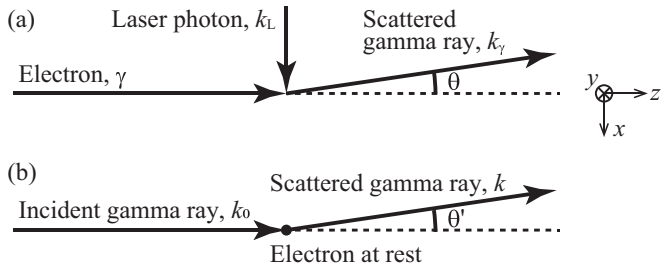

FIG. 1. Schematic illustration of (a) inverse Compton scattering for 90° collision and (b) Compton scattering of a gamma ray. The electron after scattering is not shown. The coordinate system used in the calculation and experiment is shown in (a). The direction of electron motion is the z axis, and the y and x axes are the vertical and horizontal directions, respectively.

A schematic illustration of inverse Compton scattering for 90° collision is shown in Fig. 1(a). The energy of generated gamma rays is defined using Eq. (1) in Ref. [31] and expressed as follows:

$$k_\gamma = \frac{k_L}{1-\beta\cos\theta + k_L(1-\sin\theta)/(\gamma m_e c^2)} \simeq \frac{2\gamma^2 k_L}{1+\gamma^2\theta^2}. \quad (1)$$

The final expression in Eq. (1) is derived from the limit $2\gamma k_L/m_e c^2 \ll 1$, $\theta \ll 1$, and $\beta \sim 1$. Here, k_L is the energy of the incident laser; $m_e c^2$ is the electron energy at rest, and $\beta = v/c$ is the normalized velocity of the electron, where v is the electron velocity and c is the speed of light.

B. Spatial polarization distribution and spatial intensity distribution of gamma rays generated by inverse Compton scattering

As inverse Compton scattering is equivalent to Compton scattering when it is viewed in an electron rest frame, the differential scattering cross section of inverse Compton scattering is derived using the Lorentz transformation of Compton scattering [32]. A schematic illustration of Compton scattering is shown in Fig. 1(b). The differential scattering cross section of Compton scattering of a circularly polarized gamma ray is expressed by using the Klein-Nishina formula [33],

$$\frac{d\sigma_{CS}}{\sin\theta' d\theta'} = \pi r_0^2 \left(\frac{k}{k_0}\right)^2 \left(\frac{k}{k_0} + \frac{k_0}{k} - 1 + \cos^2\theta'\right). \quad (2)$$

Here, σ_{CS} is the cross section of Compton scattering, r_0 is the classical electron radius, k_0 and k are the initial and final energies of the gamma rays, and θ' is the angle of the scattered gamma ray with regard to the incident gamma rays. The Lorentz transformation of a laser photon incident at 90° to the direction of electron motion can be calculated as follows in accordance with the calculation for 0° incidence [32]:

$$\frac{d\sigma_{CS}}{\sin\theta d\theta} = \frac{\beta(\sin\theta - 1) + \cos\theta}{\gamma^2(1-\beta\cos\theta)^2\sin\theta} \times \pi r_0^2 R^2 \left\{R + \frac{1}{R} - 1 + \cos^2\theta^{ER}\right\}, \quad (3)$$

where

$$\frac{1}{R} = 1 + \frac{\gamma k_{\mathrm{L}}}{m_{\mathrm{e}}c^2}(1 + \cos\theta^{\mathrm{ER}}) \tag{4}$$

and

$$\cos\theta^{\mathrm{ER}} = \frac{1 - \sin\theta}{\gamma^2(1 - \beta\cos\theta)} - 1 \simeq \frac{1 - \gamma^2\theta^2}{1 + \gamma^2\theta^2}. \tag{5}$$

The last term in Eq. (5) is derived from the limit $\theta \ll 1$ and $\beta \sim 1$. The intensity of gamma rays is expressed as the product of the scattering cross section and luminosity, where luminosity is independent of the Lorentz factor and scattering angle. Therefore, the differential scattering cross section indicates the spatial intensity distribution of inverse-Compton-scattered gamma rays.

The degree of circular polarization of Compton-scattered gamma rays can be calculated by deriving the Stokes parameter with reference to Sec. II B 2 in Ref. [33]. The Lorentz transformation expression for the degree of circular polarization is derived as follows:

$$\frac{P_3}{I} = \frac{(R + 1/R)\cos\theta^{\mathrm{ER}}}{R + 1/R - 1 + \cos^2\theta^{\mathrm{ER}}}, \tag{6}$$

where I is the total intensity and P_3 indicates the relative intensity of circular polarization. In this paper, the notation of the helicity of circular polarization follows the field of optics (Sec. 7.2 in [34]). Equation (6) is consistent with Eq. (5) in Ref. [17].

Figure 2 shows the spatial distribution of the intensity and Stokes parameter in the x-y plane calculated using Eqs. (3) and (6). Here, we use the following parameters: $\gamma = 1468$ and $k_{\mathrm{L}} = 1.55$ eV. These parameters are consistent with the experimental conditions at UVSOR-III. As shown in Figs. 2(a) and 2(b), gamma rays are concentrated in the area below angle $1/\gamma$. The degree of circular polarization of gamma rays is more than 90% of the left-hand circular polarization at a scattering angle of $\theta < 0.5/\gamma$ [Fig. 2(d)]. As described in the Introduction, the degree of circular polarization decreases with the increase of the scattering angle. Polarization changes from circular to linear polarization at an angle of $\theta = 1/\gamma$. Furthermore, polarization changes to right-hand circular polarization at a greater scattering angle of $\theta > 1/\gamma$.

In the case of UVSOR-III, $1/\gamma = 0.681$ mrad. This angle corresponds to a displacement of 5.0 mm at a distance of 7.3 m from the gamma-ray generation point. Therefore, the spatial polarization distribution of gamma rays can be simply measured by using a scanning collimator of 1 mm in diameter, as indicated by the small black circles in Fig. 2(c). By contrast, as the electron beam energy increases to several GeV, the $1/\gamma$ angle decreases. Consequently, measuring the spatial polarization distribution using a collimator becomes difficult.

C. Lorentz transformation of electromagnetic fields

Inverse Compton scattering of head-on collisions between a high-energy electron beam and a polarized laser is commonly investigated experimentally and computationally. Our study demonstrates that circularly polarized gamma rays are also generated by inverse Compton scattering of a 90° collision in the laboratory frame. One may wonder why circularly polarized gamma rays are produced in 90° collisions, which can be explained by the Lorentz transformation of electromagnetic fields. Coordinate systems of Lorentz transformation are defined and shown in Fig. 3. Here, we define that the (x', y', z') coordinate system is moving with velocity $\mathbf{v} = c\boldsymbol{\beta}$ in the positive z direction with regard to the (x, y, z) coordinate system and (x'', y'', z'') is a rotational coordinate system with angle ζ relative to (x, y, z). If the vector potential of the circularly polarized electromagnetic field traveling along the $-z''$ axis is defined as $\mathbf{a}'' = (a_{x''}\mathbf{e}_{x''} + a_{y''}\mathbf{e}_{y''})$, where $\mathbf{e}_{x''}$ and $\mathbf{e}_{y''}$ are the unit vectors along the x'' and y'' axes, respectively, then the electric and magnetic fields in the (x, y, z) coordinate system can be described as follows:

$$\mathbf{E} = -\frac{\partial a_{x''}}{\partial t}\cos\zeta\,\mathbf{e}_x - \frac{\partial a_{y''}}{\partial t}\mathbf{e}_y + \frac{\partial a_{x''}}{\partial t}\sin\zeta\,\mathbf{e}_z \tag{7}$$

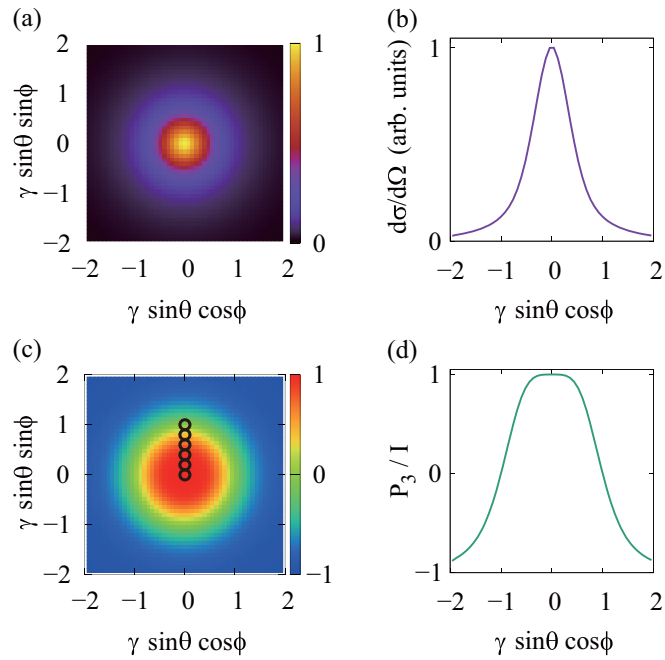

FIG. 2. (a) and (b) Intensity distribution and (c) and (d) Stokes parameters of circularly polarized gamma rays calculated using Eqs. (3) and (6). (a) and (c) indicate the spatial distribution in the x-y plane, and (b) and (d) are the line distributions along the x axis. ϕ is the azimuthal angle in the x-y plane. The calculated parameters are $\gamma = 1468$ and $k_{\mathrm{L}} = 1.55$ eV. The small black circles in (c) indicate the positions where the 1-mm-diameter collimator is scanned in the experiment.

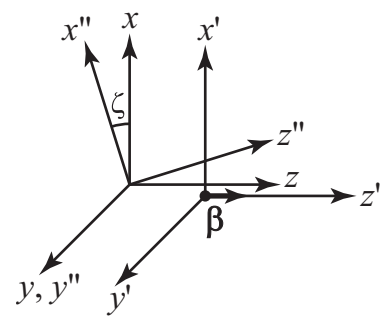

FIG. 3. Coordinate systems of Lorentz transformation.

and

$$\mathbf{B} = -\frac{\partial a_{y''}}{\partial z''}\cos\zeta\,\mathbf{e}_x + \frac{\partial a_{x''}}{\partial z''}\mathbf{e}_y + \frac{\partial a_{y''}}{\partial z''}\sin\zeta\,\mathbf{e}_z. \quad (8)$$

Here, t is the time, and $\mathbf{e}_x$, $\mathbf{e}_y$, and $\mathbf{e}_z$ are the unit vectors along the x, y, and z axes, respectively. An example of the vector potential can be found in Ref. [35]. Based on the Lorentz transformation of electromagnetic fields described in Sec. 11.10 in [34], the electric fields in the (x', y', z') coordinate system will be defined as follows:

$$E_{x'} = \gamma(E_x - c\beta B_y) = -\gamma(\beta + \cos\zeta)\frac{\partial a_{x''}}{\partial t}, \quad (9)$$

$$E_{y'} = \gamma(E_y + c\beta B_x) = -\gamma(1 + \beta\cos\zeta)\frac{\partial a_{y''}}{\partial t}, \quad (10)$$

and

$$E_{z'} = E_z = \sin\zeta\,\frac{\partial a_{x''}}{\partial t}. \quad (11)$$

Here, $\partial/\partial z'' = \partial/c\partial t$. Based on Eqs. (9) and (10), the electric fields of the laser in an electron rest frame are circularly polarized under the condition that $\beta \simeq 1$. Therefore, although a circularly polarized laser is injected from a 90° direction into an electron beam in a laboratory frame, circularly polarized gamma rays are generated.

D. Magnetic Compton scattering

The differential scattering cross section of magnetic Compton scattering can be described as [36]

$$\frac{d\sigma_{\rm CS}}{\sin\theta' d\theta'} + P\frac{d\sigma_{\rm MCS}}{\sin\theta' d\theta'} = \pi r_0^2\left(\frac{k}{k_0}\right)^2\left\{\frac{k}{k_0} + \frac{k_0}{k} - 1 + \cos^2\theta' - P(1-\cos\theta')\cos\theta'\frac{k_0+k}{m_e c^2}\right\}, \quad (12)$$

where P is the product of the degrees of polarization of the gamma ray and electron. It is positive for a left-hand circularly polarized gamma ray and an electron spin parallel to k_0. $\sigma_{\rm MCS}$ provides the polarization and spin-dependent term of the cross section for magnetic Compton scattering. The cross section integrated over the solid angle is expressed as follows [36,37]:

$$\sigma_{\rm CS} + P\sigma_{\rm MCS} = 2\pi r_0^2\left[\frac{1+\alpha}{(1+2\alpha)^2} + \frac{2}{\alpha^2} - \frac{1+\alpha}{\alpha^3}\ln(1+2\alpha) + \frac{1}{2\alpha}\ln(1+2\alpha) + P\left\{\frac{1+4\alpha+5\alpha^2}{\alpha(1+2\alpha)^2} - \frac{1+\alpha}{2\alpha^2}\ln(1+2\alpha)\right\}\right], \quad (13)$$

where $\alpha = k_0/m_e c^2$.

The analyzing power indicating the gamma-ray transmission asymmetry is defined as $(T_{\uparrow\uparrow} - T_{\uparrow\downarrow})/(T_{\uparrow\uparrow} + T_{\uparrow\downarrow})$. Here, $T_{\uparrow\uparrow,\uparrow\downarrow} = \exp(-DL\mu_{\uparrow\uparrow,\uparrow\downarrow})$; D and L are the density and length of the magnetized material, and $\mu_{\uparrow\uparrow,\uparrow\downarrow}$ is the attenuation coefficient, which is expressed as follows:

$$\mu_{\uparrow\uparrow,\uparrow\downarrow} = (\sigma_{\rm PE} + \sigma_{\rm CS} + P\sigma_{\rm MCS} + \sigma_{\rm Co} + \sigma_{\rm PP})N_A/A. \quad (14)$$

Here, subscripts indicate that P is positive or negative. $\sigma_{\rm PE}$ is the cross section of the photoelectric effect, $\sigma_{\rm Co}$ is the cross section of coherent scattering, $\sigma_{\rm PP}$ is the cross section of pair production, N_A is Avogadro's constant, and A is the atomic weight. The calculated analyzing power for magnetized iron is shown in Fig. 4. The calculated parameters are consistent with the magnetized iron used in the experiment. $\sigma_{\rm PE}$, $\sigma_{\rm Co}$, and $\sigma_{\rm PP}$ are calculated using the empirical formula described in Ref. [38], and $\sigma_{\rm CS}$ and $\sigma_{\rm MCS}$ are calculated using Eq. (13). The degree of electron spin is set to 0.061, the detailed calculation of which is described in Sec. III B. As shown in Fig. 4, for linear polarization with $P = 0$, no asymmetry appears, whereas for circular polarization with $P \neq 0$, asymmetry is measured. Therefore, as the analyzing power clearly varies depending on the magnitude and sign of P, the polarization of the gamma-ray incident on the magnetized iron can be measured by measuring the analyzing power.

E. EGS5 simulation

The EGS5 Monte Carlo simulation code [39] is used to calculate the gamma-ray energy spectra at the detectors and compare them with the measured spectra. In the simulation, the initial energy, position, and angle of the gamma rays were defined, and the energy distribution absorbed in each detector was calculated in a material configuration simulating the experiment. The energy and intensity of the inverse-Compton-scattered gamma rays were defined using Eqs. (1) and (3), and the initial position and angle were the same as those of the electron beam circulating in the UVSOR-III storage ring [40]. The relative uncertainty in the energy of the inverse-Compton-scattered gamma rays caused by the energy spread

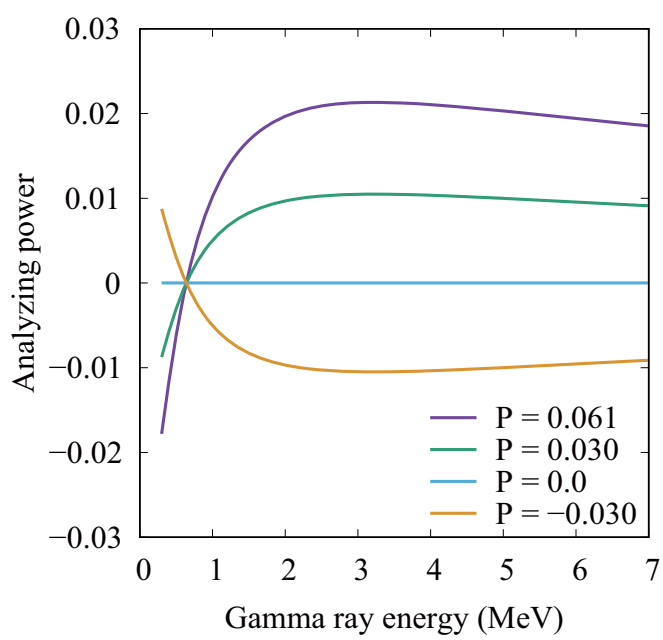

FIG. 4. Calculated analyzing power under the following conditions: $L = 65$ mm, $A = 57.35$, and $D = 8.2$ g/cm^3.

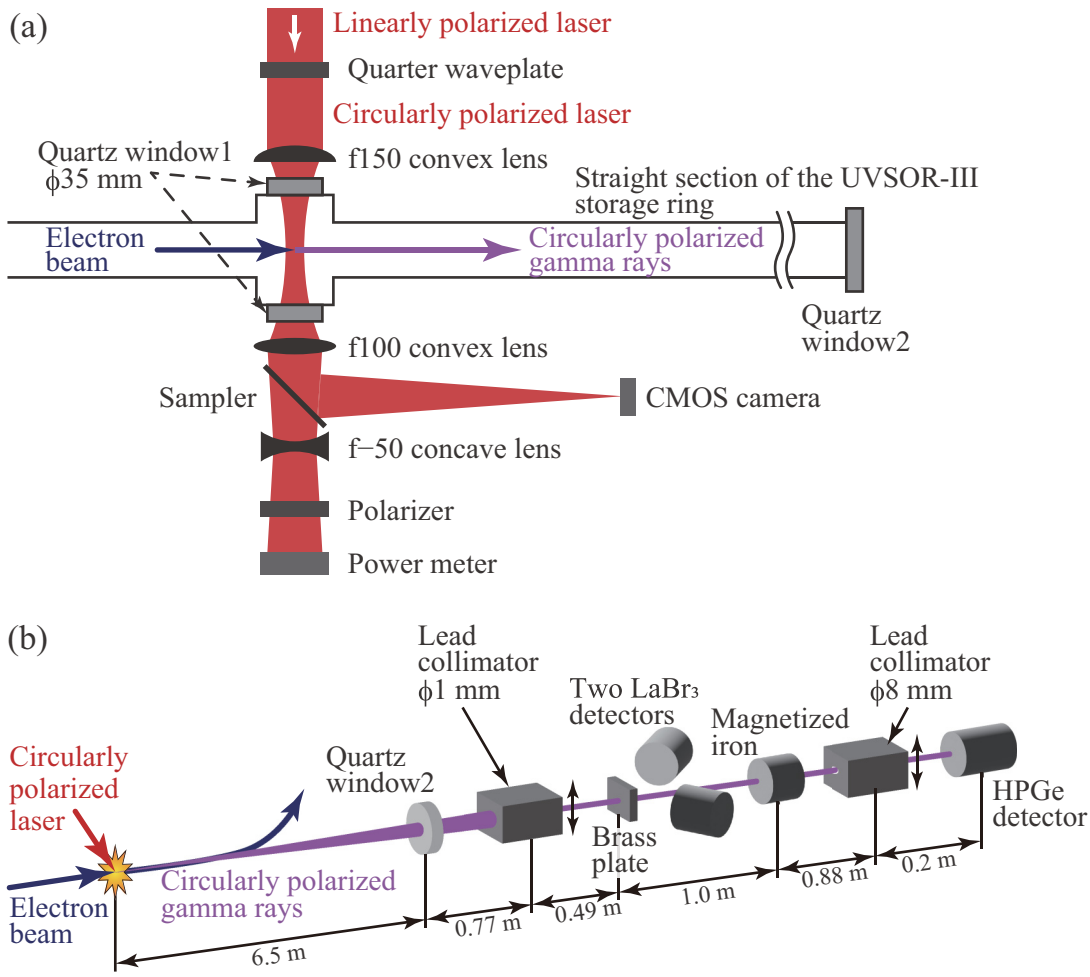

FIG. 5. (a) Detailed top view of laser injection into the vacuum duct and polarization control. (b) Schematic illustration of the spatial polarization measurement of circularly polarized gamma rays. After colliding the laser, the electron beam was bent in its direction by using a bending magnet, which was placed between the collision point and quartz window 2. The transmission of gamma rays through the magnetized iron was measured while moving the 1- and 8-mm-diameter collimators in the vertical direction.

of the electron beam and the linewidth of the laser given in Table 1 of Ref. [13] were also included in the simulation.

III. MEASUREMENT

A. Generation of a circularly polarized laser

A schematic illustration of the experiment is shown in Fig. 5. Details of the laser injection and polarization control are shown in Fig. 5(a). The Ti:sapphire laser was injected inside the vacuum duct through a quartz window attached to part of the storage ring. A lens with a focal length of 150 mm was installed in front of the quartz window to focus the laser at the electron beam collision point. The laser profile at the collision point was imaged on a complementary metal-oxide semiconductor (CMOS) camera by a lens with a focal length of 100 mm.

Laser polarization is converted from linear to circular using a quarter wave plate installed in front of the focusing lens. The angle of the wave plate generating circular polarization was determined as follows. First, the polarization axis of the linearly polarized laser entering the vacuum duct was measured by the change in power caused by the rotation of the polarizer without a wave plate [Fig. 6(a)]. The polarizer was mounted on a rotating stage and placed behind the imaging lens [Fig. 5(a)]. In avoiding damage to the polarizer, a concave lens with a focal length of −50 mm was used to widen the laser size. Next, the polarizer was rotated 90° with regard to the polarization axis of the linearly polarized laser, and the change in power was measured while rotating the wave plate [Fig. 6(b)]. The angle of the wave plate at which the power was maximum was defined as the angle at which the laser was circularly polarized. As shown in Fig. 6(c), a circularly polarized laser with a polarization of 0.9971 ± 0.0001 was generated. The fast axis of the wave plate was preliminarily confirmed using the method described in Ref. [41]. The helicity of the circularly polarized laser was fixed to the right hand throughout the experiment. Thus, the helicity of the gamma rays was left-hand circular polarization.

B. Generation of circularly polarized gamma rays and measurement of their spatial polarization distribution

A schematic illustration of the spatial polarization distribution measurement is shown in Fig. 5(b). The circularly

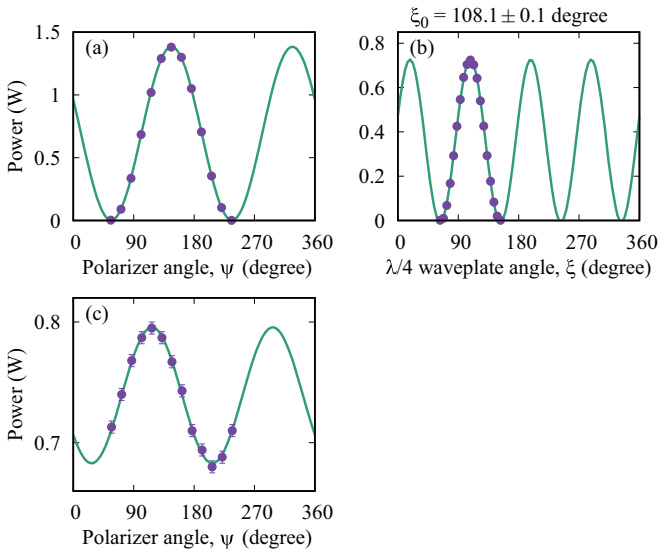

FIG. 6. (a) Laser power measured while rotating the polarizer without the quarter wave plate. The extinction ratio of the polarizer at a wavelength of 800 nm is 10^4. The purple dots indicate the measured data, and the solid line shows the fitting of the function $a_1[1 + \delta_p \cos\{2(\psi - \psi_0)\}]$, where a_1 is the coefficient, δ_p is the degree of linear polarization, ψ is the polarizer angle, and ψ_0 is the polarization axis of the linearly polarized laser. (b) Laser power measured while rotating the quarter wave plate. The purple dots are measured data, and the solid line shows the fitting of the function $a_2 \cos^2\{2(\xi - \xi_0)\}$, where a_2 is the coefficient, ξ is the wave-plate angle, and ξ_0 is the fast or slow axis of the wave plate. The uncertainty of the measured value is less than the size of the symbols. (c) Laser power measured while rotating the polarizer. The measurement was performed by removing the sampler because it has different transmittances for s and p polarization. The same fitting as in (a) was performed, and $\delta_p = 0.0761 \pm 0.0012$. Thus, the degree of circular polarization of the laser, $\sqrt{1 - \delta_p^2}$, was evaluated to be 0.9971 ± 0.0001.

polarized gamma rays were generated by injecting the circularly polarized laser into the electron beam from horizontal 90° direction. The laser was operated synchronously with the rf acceleration cavity of the storage ring [31]. As the revolution frequency of an electron bunch was 5.63 MHz and the repetition rate of the laser was 1 kHz, the electron bunch collided with the laser every 5632 laps. The parameters of the electron beam were as follows: energy = 750 MeV; energy spread in FWHM = 1.23×10^{-3}; bunch current = 30 mA; horizontal and vertical beam sizes in FWHM at the collision point = 1.3 and 0.05 mm, respectively; and bunch length in FWHM = 640 ps. The parameters of the laser were as follows: wavelength = 800 nm, linewidth in FWHM = 11 nm, pulse energy = 2 mJ, beam size in FWHM at the collision point = 15 μm, and pulse width in FWHM = 1.8 ps.

The maximum gamma ray energy, calculated pulse width, and its estimated intensity at the generation point were 6.6 MeV, 5 ps (FWHM), and 2×10^5 photons/s, respectively. The generated circularly polarized gamma rays were passed through a quartz window that divided the vacuum and atmosphere and then through a 180-mm-long lead collimator with a diameter of 1 mm. The gamma-ray intensity incident on the magnetized iron was monitored by measuring the gamma rays scattered from a brass plate placed immediately after the 1-mm-diameter collimator with two $LaBr_3$ scintillation detectors. The brass plate was 15 mm thick and 50 mm^2. The sizes of the two $LaBr_3$ scintillators were 101.6 and 88.9 mm in diameter and 127 and 101.6 mm in length. The $LaBr_3$ detectors were placed at a distance of 60 mm from the brass plate with a scattering angle of 45°. Then, the gamma rays passed through the magnetized iron with a length of 65 mm and diameter of 80 mm. The magnetized iron consisted of an iron-cobalt alloy Permendur core wound with 500 turns of conducting wire. The magnetic flux density was simulated with FEMTET (produced by Murata Software Co.), and the average magnetization along the gamma-ray transmission axis at the center of core M was estimated to be 1.34×10^6 A/m at a current of 3.98 A. The maximum magnetization of the Permendur core reaches 1.87×10^6 A/m [42], but the average value of magnetization is smaller because the magnetic flux density along the gamma-ray axis is not uniform. The average spin polarization of electrons in the material is expressed as [43]

$$P_e = M \frac{(g' - 1)2}{(g - 1)g'} \frac{1}{N_e \mu_B}, \tag{15}$$

where g (= 2.002) is the electron's g factor, g' is the gyromagnetic factor for the material, and μ_B is the Bohr magneton, $N_e = N_A DZ/A$ is the density of electrons in the material, and Z is the atomic number. Using the Permendur properties $g' = 1.92$ [44], $D = 8.2$ g/cm^3 [42], and $A = 57.35$, one obtains $P_e = 0.061$. During the experiment, the magnitude of the current was kept constant, and only the direction was changed. Therefore, the magnitude of the electron spin was constant, and only the sign was changed. Gamma rays transmitted through the magnetized iron were measured using a high-purity germanium (HPGe) detector 90.3 mm in diameter and 83.5 mm in length with a relative efficiency of 152% at 1.332 MeV. A lead collimator with a thickness of 200 mm and diameter of 8 mm was placed between the magnetized iron and HPGe detector to avoid detecting scattered gamma rays at the magnetized iron.

The alignment of the 1- and 8-mm-diameter collimators with the gamma-ray beam axis was performed as follows. First, gamma rays transmitted through the 1-mm-diameter collimator without a brass plate, magnetized iron, and 8-mm collimator were measured using the HPGe detector. The collimator was moved in 0.5-mm steps in the x and y directions, and it was aligned at the position of the maximum gamma-ray intensity. Next, synchrotron radiation generated from the bending magnet was passed through the aligned 1-mm-diameter collimator, and the center of the 8-mm-diameter collimator was aligned with the synchrotron radiation.

The measurements of spatial polarization distribution were performed as follows. Energy spectra of $LaBr_3$ and HPGe detectors were measured in the positive and negative directions of the magnetized iron current, respectively. Then, the background spectra for the $LaBr_3$ detectors were measured by removing the brass plate. The measurement times for all three types of measurements were the same, and this measurement routine was considered to be one set. This one set of measurements was repeated multiple times. Measurements without

laser injection were also taken in each direction of the magnetized iron current, which were used as background spectra for the HPGe detector. The number of repeated measurements, the measurement time for one set, and the measurement times without the laser are shown in Table I. The angular spread of the electron beam circulating in the storage ring is smaller in the vertical direction than in the horizontal one. In the case of UVSOR-III, the angular spread of the electron beam is approximately ±0.05 mrad in the horizontal direction and ±0.01 mrad in the vertical direction. Hence, in reducing the effect of the angular spread of the electron beam, measurements were taken by moving the 1- and 8-mm-diameter collimators in 1-mm steps in the vertical axis.

IV. RESULTS AND DISCUSSION

A. Energy spectra of gamma rays measured using $LaBr_3$ and HPGe detectors

The measured energy spectra subtracted background and calculated energy spectra using EGS5 are shown in Fig. 7. The energy resolutions of the HPGe detector and $LaBr_3$ detector were computed to be 0.2% and 2% in FWHM, respectively. The calculated energy spectra of $LaBr_3$ are consistent with the measured results. On the contrary, the calculated energy spectrum of HPGe is consistent with the measurement results in the region below the maximum energy where the intensity is strongest, for example, below 6.6 MeV at the 0-mm collimator position. However, the measurement results in the higher-energy region do not agree with the calculated energy spectra. This difference in results is due to the pileup effect in which two or more gamma rays are detected simultaneously within the time resolution of the HPGe detector. The more intense the gamma rays per pulse are, the more likely it is that the pileup will occur.

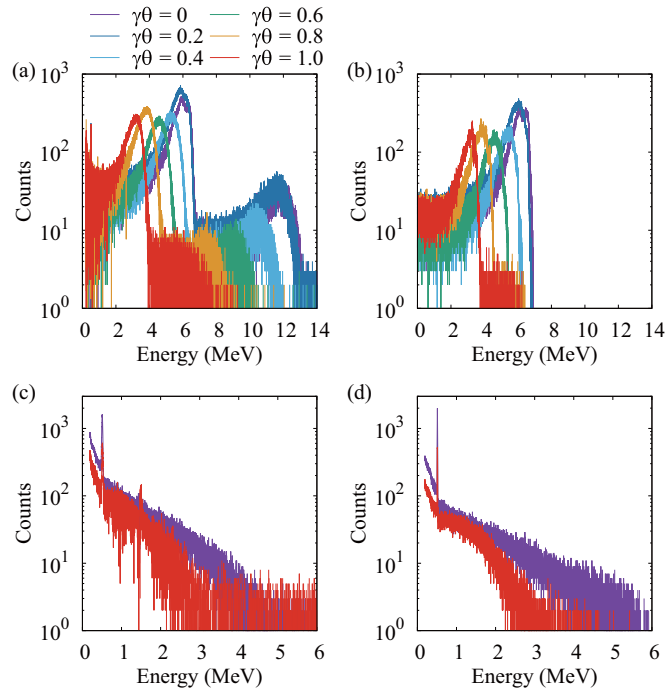

FIG. 7. (a) Measured and (b) calculated energy spectra of gamma rays transmitted through the magnetized iron measured using the HPGe detector. (c) Measured and (d) calculated energy spectra of gamma rays scattered from the brass plate measured using $LaBr_3$ detectors. The energy-spectrum-subtracted backgrounds are displayed in (a) and (c). The position of the collimator is shown. The energy spectra of $LaBr_3$ are shown only for collimator positions of $\gamma\theta = 0$ and 1.

B. Analyzing power

In calculating the analyzing power, $T_{\uparrow\uparrow,\uparrow\downarrow}$ was defined as follows:

$$T_{\uparrow\uparrow,\uparrow\downarrow} = \frac{M_{\uparrow\uparrow,\uparrow\downarrow}}{N_{\uparrow\uparrow,\uparrow\downarrow}}. \tag{16}$$

Here, $M_{\uparrow\uparrow,\uparrow\downarrow}$ and $N_{\uparrow\uparrow,\uparrow\downarrow}$ are the total counts of energy spectra measured using the HPGe detector, and the $LaBr_3$ detectors subtracted the background.

The total counts of the HPGe detector corrected for pileup effects were calculated using the following method. As described in Ref. [45], the probability distribution of the number of scattered gamma-ray photons per pulse n follows a Poisson distribution $P_m(n)$, where m is the average number of scattered photons per pulse. Here, let ϵ denote the total detection efficiency of the HPGe detector; the number of single- and double-photon detections per pulse is described as follows:

$$M_1 = P_m(1)\epsilon + P_m(2)2\epsilon(1-\epsilon) \tag{17}$$

TABLE I. Measurement conditions and analysis parameters for each collimator position. The number of repeated measurements and the measurement time per one set for each collimator position are shown in the third and fourth columns. Measurement time without laser is shown in the fifth column. The analysis parameters ϵ, k_{HPGe}, and k_{LaBr_3} are shown in the last three columns.

Collimator position (mm)	$\gamma\theta$	Number of repeated measurements	Measurement time for one set (min)	Measurement time without the laser (min)	Total detection efficiency ϵ	k_{HPGe} (MeV)	k_{LaBr_3} (MeV)
0	0.0	2	90	30	0.76	6.62	5.2
1	0.2	3	90	30	0.76	6.55	5.2
2	0.4	1	180	30	0.76	6.07	4.9
3	0.6	1	270	30	0.76	5.30	4.4
4	0.8	4	150	30	0.77	4.45	3.8
5	1.0	5	150	60	0.79	3.67	3.2

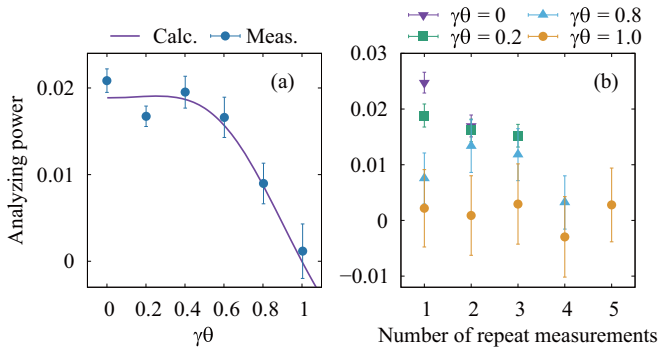

FIG. 8. (a) Measured and calculated analyzing power at each scattering angle. The solid line is the result of the calculation using Eqs. (6) and (14) with P in Eq. (14) being $P = P_3/I \times P_e = P_3/I \times 0.061$. (b) Measured analyzing power in individual measurements. The position of the collimator is seen. The uncertainty of the measurements was calculated by the propagation of statistical errors.

and

$$M_2 = P_m(2)\epsilon^2. \tag{18}$$

Therefore,

$$P_m(1) + P_m(2) = M_1\frac{1}{\epsilon} - M_2\frac{2(1-\epsilon)}{\epsilon^2} + M_2\frac{1}{\epsilon^2}. \tag{19}$$

The total counts of the HPGe detector were calculated using Eq. (19), with M_1 being the total counts ranging from 2.0 to k_{HPGe} MeV of the energy spectrum and M_2 being the total counts ranging from $k_{\mathrm{HPGe}} + 0.5$ to $2k_{\mathrm{HPGe}}$ MeV. The values of k_{HPGe} are listed in Table I, and they were determined from the maximum energy of the gamma ray at each collimator position calculated using Eq. (1). The total detection efficiency at each collimator position was calculated using GEANT4 [46], and the result is listed in Table I. The background counts without laser injection were calculated as the sum of the count values over the same range.

The total counts of $LaBr_3$ indicated the sum of count values for the range of 0.2 to $k_{\mathrm{LaBr_3}}$ MeV, excluding 1.3–1.6 MeV, which corresponds to the ^{40}K energy region of the environmental radiation. $k_{\mathrm{LaBr_3}}$ was the maximum energy of gamma rays incident on the $LaBr_3$ detectors from the brass plate, calculated using the theoretical equation for Compton scattering (Table I). As the minimum energy of Compton-scattered gamma rays incident on the $LaBr_3$ detectors from the brass plates was 0.5 MeV, the lower limit for the calculation of the total counts was set to 0.2 MeV. Figure 8 shows the results for the measured and calculated analyzing power at each collimator position.

C. Discussion

As shown in Fig. 8(a), the sign of the measured analyzing power is positive, indicating that the helicity of the generated circularly polarized gamma rays is left hand, as expected. Furthermore, the amount of change in the analyzing power with the scattering angle is consistent with the calculated results. Theoretically, the polarization of the gamma rays is circular in the range $\gamma\theta < 0.5$ and linear at $\gamma\theta = 1$. On the contrary, in the case of linearly polarized gamma rays generated by inverse Compton scattering of the linearly polarized laser, their spatial polarization distribution was measured at NewSUBARU [47]. The polarization axis of linearly polarized gamma rays rotates with the scattering angle. In our measurement, the polarization axis of the linearly polarized part of $\gamma\theta = 1$ can be measured, but it is left for future work as the measurement takes a lot of time because of the low intensity of gamma rays.

V. CONCLUSIONS

The spatial polarization distribution of circularly polarized gamma rays generated by 90° collisional inverse Compton scattering of a circularly polarized laser was measured using magnetic Compton scattering. Gamma rays with an energy of 6.6 MeV were collimated using a 1-mm-diameter collimator and irradiated onto magnetized iron. The transmission of gamma rays to magnetized iron was measured using $LaBr_3$ scintillation and HPGe detectors, and the asymmetry of the transmission was measured by reversing the direction of the electron spin of the magnetized iron. Asymmetry changes with the polarization of the gamma ray; thus, the polarization of the incident gamma rays can be measured. For the HPGe detector, the effect of pileup was corrected. By scanning the collimator in the vertical direction, the polarization of the gamma rays was circular at the central axis, which changed to elliptical as the scattering angle increased and became linearly polarized at an angle of $1/\gamma$. Although the laser is 100% circularly polarized, the polarization of the gamma rays changes with the scattering angle. Theoretical calculations of the transmittance were performed, and the results were consistent with the measurements. In utilizing gamma rays with high circular polarization, a collimator can be used to cut out only the central axis within a scattering angle of $0.5/\gamma$. In addition, this result indicated that circularly polarized gamma rays were generated by 90° collisional inverse Compton scattering of high-energy electron beams with circularly polarized lasers.

ACKNOWLEDGMENTS

Y.T. would like to thank Dr. S. Miyamoto at the Osaka University for a helpful discussion. This work was performed at the BL1U of UVSOR Synchrotron Facility at the Institute for Molecular Science (IMS program 22IMS6604) and was supported by JSPS KAKENHI Grants No. 21H03740 and No. 21K04950.

[1] H. Ohgaki, T. Noguchi, S. Sugiyama, T. Yamazaki, T. Mikado, M. Chiwaki, K. Yamada, R. Suzuki, and N. Sei, Linearly polarized photons from Compton backscattering of laser light for nuclear resonance fluorescence experiments, Nucl. Instrum. Methods Phys. Res., Sect. A **353**, 384 (1994).

[2] S. Y. Ryu *et al.* (LEPS Collaboration), Interference Effect between ϕ and $\Lambda(1520)$ Production Channels in the $\gamma p \to K^+K^-p$ Reaction near Threshold, Phys. Rev. Lett. **116**, 232001 (2016).

[3] J. Ahrens *et al.* (GDH and A2 Collaborations), First Measurement of the Gerasimov-Drell-Hearn Integral for ^{1}H from 200 to 800 MeV, Phys. Rev. Lett. **87**, 022003 (2001).

[4] A. I. Titov, M. Fujiwara, and K. Kawase, Parity nonconservation in nuclear excitation by circularly polarized photon beam, J. Phys. G **32**, 1097 (2006).

[5] T. Omori, M. Fukuda, T. Hirose, Y. Kurihara, R. Kuroda, M. Nomura, A. Ohashi, T. Okugi, K. Sakaue, T. Saito, J. Urakawa, M. Washio, and I. Yamazaki, Efficient Propagation of Polarization from Laser Photons to Positrons through Compton Scattering and Electron-Positron Pair Creation, Phys. Rev. Lett. **96**, 114801 (2006).

[6] G. Alexander *et al.*, Observation of Polarized Positrons from an Undulator-Based Source, Phys. Rev. Lett. **100**, 210801 (2008).

[7] M. Fukuda, T. Aoki, K. Dobashi, T. Hirose, T. Iimura, Y. Kurihara, T. Okugi, T. Omori, I. Sakai, J. Urakawa, and M. Washio, Polarimetry of Short-Pulse Gamma Rays Produced through Inverse Compton Scattering of Circularly Polarized Laser Beams, Phys. Rev. Lett. **91**, 164801 (2003).

[8] O. F. Kulikov, Y. Y. Telnov, E. I. Filippov, and M. N. Yakimenko, Compton effect on moving electrons, Phys. Lett. **13**, 344 (1964).

[9] C. Bemporad, R. H. Milburn, N. Tanaka, and M. Fotino, High-energy photons from Compton scattering of light on 6.0-GeV electrons, Phys. Rev. **138**, B1546 (1965).

[10] K. T. Phuoc, S. Corde, C. Thaury, V. Malka, A. Tafzi, J. P. Goddet, R. C. Shah, S. Sebban, and A. Rousse, All-optical Compton gamma-ray source, Nat. Photonics **6**, 308 (2012).

[11] C. Liu, G. Golovin, S. Chen, J. Zhang, B. Zhao, D. Haden, S. Banerjee, J. Silano, H. Karwowski, and D. Umstadter, Generation of 9 MeV γ-rays by all-laser-driven Compton scattering with second-harmonic laser light, Opt. Lett. **39**, 4132 (2014).

[12] S. H. Park, V. N. Litvinenko, W. Tornow, and C. Montgomery, Spatial distribution and polarization of γ-rays generated via Compton backscattering in the Duke/OK-4 storage ring FEL, Nucl. Instrum. Methods Phys. Res., Sect. A **475**, 425 (2001).

[13] C. Sun and Y. K. Wu, Theoretical and simulation studies of characteristics of a Compton light source, Phys. Rev. Spec. Top.–Accel. Beams **14**, 044701 (2011).

[14] V. Petrillo, A. Bacci, C. Curatolo, I. Drebot, A. Giribono, C. Maroli, A. R. Rossi, L. Serafini, P. Tomassini, C. Vaccarezza, and A. Variola, Polarization of x-gamma radiation produced by a Thomson and Compton inverse scattering, Phys. Rev. Spec. Top.–Accel. Beams **18**, 110701 (2015).

[15] Z. Chi, Polarization transfer from a laser to x rays via Thomson scattering with relativistic electrons: A dipole radiation perspective, J. Appl. Phys. **128**, 244904 (2020).

[16] F. R. Arutyunyan and V. A. Tumanyan, Quasi-monochromatic and polarized high-energy gamma rays, Sov. Phys. Usp. **7**, 339 (1964).

[17] I. I. Gol'dman and V. A. Khoze, Polarization effects in Compton scattering by relativistic electrons, Sov. Phys. JETP **30**, 501 (1970).

[18] A. M. Sandorfi, M. J. LeVine, C. E. Thorn, G. Giordano, G. Matone, and C. Schaerf, High energy gamma ray beams from Compton backscattered laser light, IEEE Trans. Nucl. Sci. **30**, 3083 (1983).

[19] D. Babusci, L. Casano, A. D'Angelo, P. Picozza, C. Schaerf, and B. Girolami, Project GRAAL: The scientific case, Nuovo Cimento A **103**, 1555 (1990).

[20] D. Babusci, G. Giordano, and G. Matone, Photon polarization properties in laser backscattering, Phys. Lett. B **355**, 1 (1995).

[21] J. P. Bocquet *et al.*, Graal: A polarized γ-ray beam at ESRF, Nucl. Phys. A **622**, c124 (1997).

[22] K. Dobashi, T. Hirose, T. Kumita, Y. Kurihara, T. Muto, T. Omori, T. Okugi, K. Sugiyama, and J. Urakawa, Generation of positrons via pair-creation from Compton scattered gamma-rays, Nucl. Instrum. Methods Phys. Res., Sect. A **437**, 169 (1999).

[23] A. D'Angelo, O. Bartalini, V. Bellini, P. L. Sandri, D. Moricciani, L. Nicoletti, and A. Zucchiatti, Generation of Compton backscattering γ-ray beams, Nucl. Instrum. Methods Phys. Res., Sect. A **455**, 1 (2000).

[24] Y. Taira, T. Hayakawa, and M. Katoh, Gamma-ray vortices from nonlinear inverse Thomson scattering of circularly polarized light, Sci. Rep. **7**, 5018 (2017).

[25] Y. Taira and M. Katoh, Generation of optical vortices by nonlinear inverse Thomson scattering at arbitrary angle interactions, Astrophys. J. **860**, 45 (2018).

[26] K. Yagi, H. Onuki, S. Sugiyama, and T. Yamazaki, Absolute spectral brightness and polarization characteristics of radiation from a polarizing undulator in the visible region, Rev. Sci. Instrum. **63**, 396 (1992).

[27] Y. Taira, R. Yamamoto, K. Sugita, Y. Okano, T. Hirade, S. Namizaki, T. Ogawa, and Y. Adachi, Development of gamma-ray-induced positron age–momentum correlation measurement, Rev. Sci. Instrum. **93**, 113304 (2022).

[28] A. Kawasuso, M. Maekawa, Y. Fukaya, A. Yabuuchi, and I. Mochizuki, Spin-polarized positron annihilation measurements of polycrystalline Fe, Co, Ni, and Gd based on Doppler broadening of annihilation radiation, Phys. Rev. B **83**, 100406(R) (2011).

[29] A. P. Potylitsin, Production of polarized positrons through interaction of longitudinally polarized electrons with thin targets, Nucl. Instrum. Methods Phys. Res., Sect. A **398**, 395 (1997).

[30] D. B. Gustavson, J. J. Murray, T. J. Phillips, R. F. Schwitters, C. K. Sinclair, J. R. Johnson, R. Prepost, and D. E. Wiser, A backscattered laser polarimeter e^+e^- storage rings, Nucl. Instrum. Methods **165**, 177 (1979).

[31] Y. Taira, M. Adachi, H. Zen, T. Tanikawa, N. Yamamoto, M. Hosaka, Y. Takashima, K. Soda, and M. Katoh, Generation of energy-tunable and ultra-short-pulse gamma rays via inverse Compton scattering in an electron storage ring, Nucl. Instrum. Methods Phys. Res., Sect. A **652**, 696 (2011).

[32] J. Stepanek, Parametric study of laser Compton-backscattering from free relativistic electrons, Nucl. Instrum. Methods Phys. Res., Sect. A **412**, 174 (1998).

[33] W. H. McMaster, Matrix representation of polarization, Rev. Mod. Phys. **33**, 8 (1961).

[34] J. D. Jackson, *Classical Electrodynamics*, 3rd ed. (Wiley, New York, 1999).

[35] E. Esarey, S. K. Ride, and P. Sprangle, Nonlinear Thomson scattering of intense laser pulses from beams and plasmas, Phys. Rev. E **48**, 3003 (1993).

[36] H. A. Tolhoek, Electron polarization, theory and experiment, Rev. Mod. Phys. **28**, 277 (1956).

[37] O. Klein and Y. Nishina, Über die Streuung von Strahlung durch freie Elektronen nach der neuen relativistischen Quantendynamik von Dirac, Z. Phys. **52**, 853 (1929).

[38] M. Noguchi, Empirical equations for photon interaction cross section and mass attenuation coefficient [in Japanese], Radioisotopes **36**, 49 (1987).

[39] H. Hirayama, Y. Namito, A. F. Bielajew, S. J. Wilderman, and W. R. Nelson, The EGS5 code system, Stanford Linear Accelerator Center, Technical Report No. SLAC-R-730, 2016 (unpublished).

[40] M. Adachi, H. Zen, T. Konomi, J. Yamazaki, K. Hayashi, and M. Katoh, Design and construction of UVSOR-III, J. Phys.: Conf. Ser. **425**, 042013 (2013).

[41] P.-C. Logofatu, Simple method for determining the fast axis of a wave plate, Opt. Eng. **41**, 3316 (2002).

[42] F. Fiorillo, G. Bertotti, C. Appino, and M. Pasquale, Soft magnetic materials, in *Wiley Encyclopedia of Electrical and Electronics Engineering* (Wiley, Hoboken, NJ, 2016), pp. 1–42.

[43] K. Aulenbacher, E. Chudakov, D. Gaskell, J. Grames, and K. D. Paschke, Precision electron beam polarimetry for next generation nuclear physics experiments, Int. J. Mod. Phys. E **27**, 1830004 (2018).

[44] G. G. Scott and H. W. Sturner, Magnetomechanical ratios for Fe-Co alloys, Phys. Rev. **184**, 490 (1969).

[45] T. Kondo, H. Utsunomiya, H. Akimune, T. Yamagata, A. Okamoto, H. Harada, F. Kitatani, T. Shima, K. Horikawa, and S. Miyamoto, Determination of the number of pulsed laser-Compton scattering photons, Nucl. Instrum. Methods Phys. Res., Sect. A **659**, 462 (2011).

[46] S. Agostinelli *et al.*, Geant4—a simulation toolkit, Nucl. Instrum. Methods Phys. Res., Sect. A **506**, 250 (2003).

[47] S. Miyamoto, Laser Compton scattering gamma-ray beam source at NewSUBARU storage ring, in *International Workshop of Laser Compton Scatter Gamma Rays at Electron Storage Rings* (unpublished).